The HiCal 2 Instrument: Calibration and Antarctic Surface Reflectivity Measurement for the ANITA Experiment

P. W. Gorham[c], P. Allison[b,k], O. Banerjee[b,k], L. Batten[i], J. J. Beatty[b,k],
K. Belov[j], D. Z. Besson[e,n], W. R. Binns[f], V. Bugaev[f], P. Cao[h], C. Chen[d],
P. Chen[d], J. M. Clem[h], A. Connolly[b,k], L. Cremonesi[i], B. Dailey[b],
C. Deaconu[l], P. F. Dowkontt[a], B. D. Fox[c], J. Gordon[b], C. Hast[g], B. Hill[c],
R. Hupe[b], M. H. Israel[f], J. Kowalski[c], J. Lam[a], J. G. Learned[c], K. M. Liewer[j],
T.C. Liu[d], A. Ludwig[l], S. Matsuno[c], C. Miki[c], M. Mottram[i], K. Mulrey[h],
J. Nam[d], R. J. Nichol[i], A. Novikov[e,n], E. Oberla[l], S. Prohira[e,*], K. Ratzlaff[e],
B. F. Rauch[f], J. Roberts[c], A. Romero-Wolf[j], B. Rotter[c], J. Russell[c],
D. Saltzberg[a], H. Schoorlemmer[c], D. Seckel[h], S. Stafford[b], J. Stockham[e],
M. Stockham[e], B. Strutt[a], K. Tatem[c], G. S. Varner[c], A. G. Vieregg[l],
S. A. Wissel[m], F. Wu[a], R. Young[e]

[a]*Dept. of Physics and Astronomy, Univ. of California, Los Angeles, Los Angeles, CA 90095.*
[b]*Dept. of Physics, Ohio State Univ., Columbus, OH 43210.*
[c]*Dept. of Physics and Astronomy, Univ. of Hawaii, Manoa, HI 96822.*
[d]*Dept. of Physics, Grad. Inst. of Astrophys.,& Leung Center for Cosmology and Particle Astrophysics, National Taiwan University, Taipei, Taiwan.*
[e]*Dept. of Physics and Astronomy, Univ. of Kansas, Lawrence, KS 66045.*
[f]*Dept. of Physics, Washington Univ. in St. Louis, MO 63130.*
[g]*SLAC National Accelerator Laboratory, Menlo Park, CA, 94025.*
[h]*Dept. of Physics, Univ. of Delaware, Newark, DE 19716.*
[i]*Dept. of Physics and Astronomy, University College London, London, United Kingdom.*
[j]*Jet Propulsion Laboratory, Pasadena, CA 91109.*
[k]*Center for Cosmology and Particle Astrophysics, Ohio State Univ., Columbus, OH 43210.*
[l]*Dept. of Physics, Enrico Fermi Institute, Kavli Institute for Cosmological Physics, Univ. of Chicago , Chicago IL 60637.*
[m]*Dept. of Physics, California Polytechnic State Univ., San Luis Obispo, CA 93407.*
[n]*National Research Nuclear University, Moscow Engineering Physics Institute, 31 Kashirskoye Highway, Russia 115409*

Abstract

The NASA supported High-Altitude Calibration (HiCal)-2 instrument flew as a companion balloon to the ANITA-4 experiment in December 2016. Based on a HV discharge pulser producing radio-frequency (RF) calibration pulses, HiCal-2 comprised two payloads, which flew for a combined 18 days, covering 1.5 revolutions of the Antarctic continent. ANITA-4 captured over 10,000 pulses

*Corresponding author

Email address: `prohira@ku.edu` (S. Prohira)

arXiv:1710.11175v1 [physics.ins-det] 30 Oct 2017

from HiCal, both direct and reflected from the surface, at distances varying from 100–800 km, providing a large dataset for surface reflectivity measurements. Herein we present details on the design, construction and performance of HiCal-2.

---

1. Introduction: The HiCal project and ANITA

The Antarctic Impulsive Transient Antenna (ANITA) [1] is a balloon-borne antenna array instrument that searches for Askaryan radio emissions from interactions of ultra-high-energy cosmic ray neutrinos with the Antarctic ice [2]. The ANITA instrument is also sensitive to ultra-high-energy cosmic ray (UHECR) radio signals, which are detected after the radio signal from the down-going shower is reflected up off of the ice surface. One important experimental uncertainty is the extent to which the surface roughness affects the received signal amplitude and spectrum of cosmic rays. The HiCal instrument is a balloon-borne pulser that follows the ANITA payload on a separate balloon and periodically emits impulsive broadband RF signals. These radio pulses can be received by ANITA twice, both direct and reflected from the Antarctic surface, simultaneously calibrating the ANITA instrument and providing measurements of the surface reflectivity at various incidence angles. The various signals of interest to which ANITA is sensitive are shown diagrammatically in Figure 1.
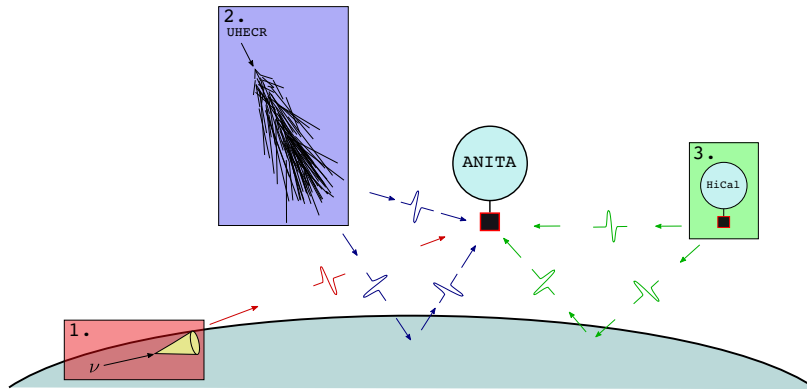

Figure 1: The various signals searched for by ANITA. 1) Upward going neutrino interactions with ice molecules create cones of Askaryan radiation, which upon exit from the ice, are detected by ANITA as short impulsive transients. 2) UHECR showers produce radio by a mix of the Askaryan effect and geomagnetic deflection, and are down-going. UHECR signals are detected by ANITA both directly, and, more commonly, after being reflected up off of the ice. 3) HiCal produces an impulsive RF signal to mimic the UHECR signal. ANITA receives the HiCal signal both direct and reflected from the ice.

HiCal-1 flew successfully in December 2014 as a companion balloon to ANITA-3 [3]. In this paper, we discuss an improved system, HiCal-2, that accompanied ANITA-4 on its circumpolar journey in December 2016.

A theoretical description of the surface reflectivity problem is given in [4], which quantifies the extent to which surface roughness can affect the reconstructed primary UHECR energy. To test this model, one can analyze the ratio of reflected vs. direct signal amplitudes of various signals as seen by the ANITA instrument. An analysis of surface reflectivity using the sun during the ANITA-2 flight is given in [5], and an analysis of satellite, solar, and HiCal-1 data during the ANITA-3 flight is given in [3]. The HiCal-1 data represented the first transient signals to be analyzed in such a way, but unfortunately the flight path only allowed for measurements at very large separation distances, indicating some discrepancy between model calculation and data at such glancing surface incidence angles. HiCal-2 was flown to provide considerably improved statistics, over a wider range of incidence angles, and investigate further the apparent disagreement between model and HiCal-1 data.

1.1. HiCal 2 subsystems

HiCal-2 consisted of 4 main sub-systems shown in Figure 2:

1. The pulse generator and antenna, inside of a 1 atmosphere Pressure Vessel (PV).
2. Telemetry, command/control, and GPS information subsystems provided by NASAs Columbia Scientific Balloon Facility (CSBF) to and from the instrument, as well as the battery power supply.
3. The Azimuth and Time-Stamp Apparatus (ATSA), for heading and environmental data.
4. The HiCal system board, which timestamped the outgoing pulses and combined PV pressure and ATSA data into packets to be telemetered .

Collectively, these systems were constrained by a 5 kg total weight limit, which proved to be an engineering challenge. Design choices had to be made to maximize performance of the instrument, while at the same time minimizing weight.
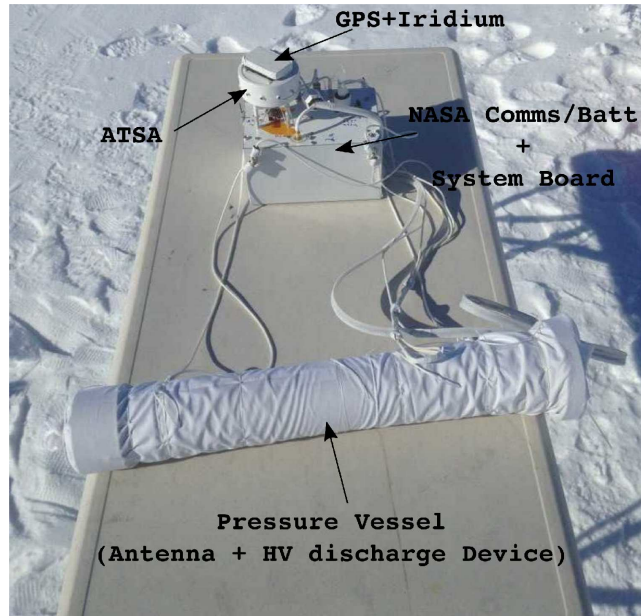
Figure 2: The HiCal 2 instrument.

2. high-voltage Pulse Generation

2.1. Piezoelectricity

"Piezoelectricity" is the term for the electric potential generated by a mechanical deformation of a particular type of crystal. Of interest in high-voltage (HV) applications is the fact that, for most crystals, there is a linear regime where the output voltage is proportional to the applied stress. A device which rapidly deforms a robust crystal, in many cases by striking the crystal with a spring-loaded hammer, can produce a potential of many kV. One such device, the MSR camp-stove lighter of Figure 3, is a particularly robust model, typically providing >100,000 "clicks" without failure of the crystal or striking mechanism. In this case, the impact of the hammer with the crystal results in an HV discharge across the ∼6 mm space between the core and the sheath of the protruding tube. The benefits of using such a device as an HV source are two-fold. One, the power required to generate the HV discharge is solely that needed to depress the clicker mechanically, which can be done using a motor and camshaft, as described below, which for HiCal 2 was 140 mW RMS. Second, the HV source itself is electrically isolated from the electromechanical operation of the "clicker", which is advantageous in a radio frequency application.

4

Figure 3: The MSR camp stove lighter.

2.2. A Model for high-voltage Discharge

The ideal HiCal pulse would resemble a delta function in time, thereby probing the Antarctic surface with equal power at every frequency. To approach this ideal, HiCal-1 implemented a standard spark-gap transmitter, as used in late 19th century radio experimentation and telegraphy. Spark-gap transmitters consist of an antenna attached either in series or in parallel to an air-gap and a high-voltage source. The high voltage source generates a potential across the air gap such that an arc occurs between its nodes. During breakdown, RF is produced and transmitted via the antenna. Spark-gap transmitters are attractive for our purposes because the resultant RF is generally highly broadband, due to its transient nature. HiCal-2 improved upon the design of a spark-gap transmitter by coupling the spark gap itself directly to the feedpoint of the antenna, as shown in Figure 8.

Empirically, we observed an inverse relationship between spark gap size and RF emission amplitude for spark gap lengths shorter than 5 mm, as shown in Figure 5. Lengths longer than this were not considered, since breakdown voltages for these lengths were out of reach for the technology tested. The amplitude of the output pulse increased as the spark gap was shortened, down to a limit of 230 μm, below which the amplitude began to drop again. This will be discussed further in the summary section.
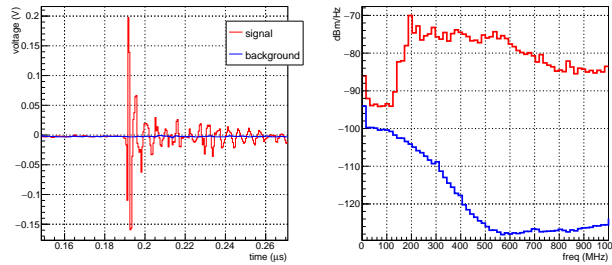
5

3. Instrument

3.1. high-voltage System

Figure 4: An example pulse from the HiCal-2 system, as received by an Anita-4 horn antenna at a distance of 40 m and read out by a 500 MHz oscilloscope, compared to ambient background. Left: time. Right: Power spectrum.
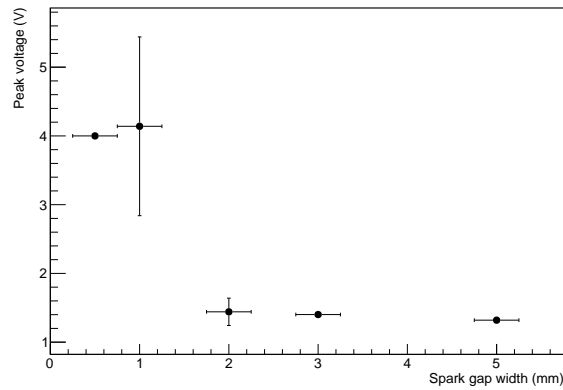

Figure 5: An inverse relationship exists between the width of a spark gap and the amplitude of the resultant pulse.

HiCal 2 implements the MSR sparker as the HV source of Figure 8. A servo motor turns a cam at a rate of ∼0.1 Hz that depresses the spring of the MSR sparker, thus generating an HV potential once per revolution, which is then transmitted to the bi-cone antenna. One half of the bi-cone is attached to the core of the sparker, the other half to the sheath. As long as the spark gap between the antenna halves is the minimum impedance path in the circuit, the breakdown location migrates from the MSR sparker core/sheath to the antenna. This breakdown causes an arc across the gap between the two halves of the bicone antenna, as shown in Figure 8. Empirical evidence suggests that

6

this initial breakdown, the rush of current at the rapid closing of the circuit, is responsible for the sharp RF discharge.

A key benefit of this system is that the primary failure mode is fairly well-defined. Because the HV generation is decoupled from the electronics that turn the motor, any electronics failure will simply result in no pulses, as opposed to an unpredictable discharge.

The MSR clicker was chosen for its durability. Several duration tests were performed to ensure that the device would continue to perform after tens of thousands of clicks, and in various environments. For one such test, the motor was run continuously for 32 hours, and the output pulses were recorded. Figure 6 shows a sigma of roughly 25% for the power variation, with a trend line that stays flat for the duration. Figure 7 shows a comparison of the first, the 24,000th, and 48,000th pulse from a 96 hour duration test. These pulses look nearly identical in both time and frequency space, demonstrating the robustness of the piezo/breakdown system.
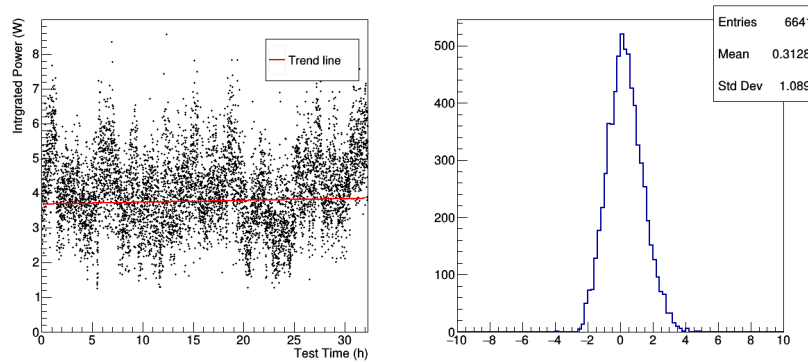

Figure 6: A 32-hour spark test, showing the consistency of the HV discharge unit. Left: the integrated power around the peak region. Right: residuals.
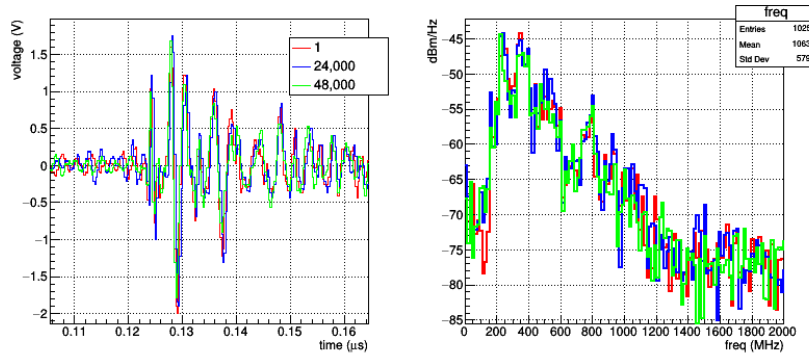

Figure 7: Comparisson of several pulses from a 90+ hour duration test, showing consistency over time. Left:time. Right: Power spectrum.

7

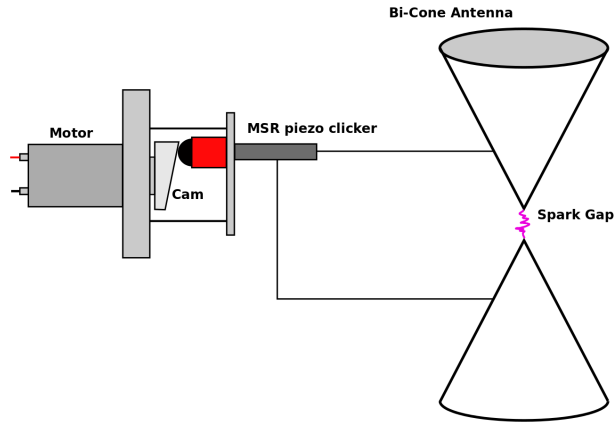Figure 8: Schematic of the motor mount, MSR piezo unit, and the bicone antenna (not to scale). The spark gap is exaggerated for conceptual purposes.

3.2. Antenna

The HiCal-2 bicone antenna of Figure 9 was subject to two design constraints. First, it needed to be as lightweight as possible. Second, it needed to have a very small, highly controlled spark gap. The antenna consists of 24 gauge aluminum sheet cut and rolled into the bicone configuration. A machined spacer, shown in Figure 9, separates the two antenna halves, insulating them from one another. Threaded into this spacer is a tunable spark gap, set to roughly 230μm. The spacer is coupled to the antenna via brass set screws. The antenna's rigidity is provided by the pressure vessel itself, with an ID matching the bicone OD for a snug fit.
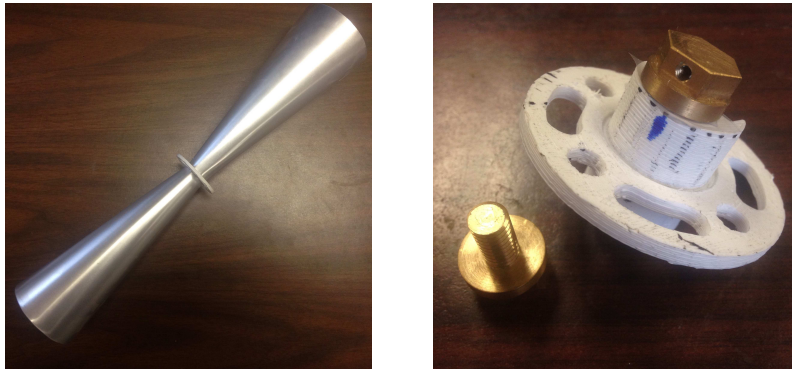

Figure 9: The HiCal-2 bicone antenna, left, with a detail of the 3d-printed spacer and machined spark gap set bolt, right.

3.3. Pressure Vessel and Timestamp System

To maintain the integrity and consistency of the breakdown, the atmosphere around the antenna must be maintained near 1000 mbar. Therefore, the HV system and antenna were housed in a 1 atm pressure vessel (PV).Weight and dielectric requirements predicated the use of a lightweight plastic. Acrylonitrile butadiene styrene (ABS), a typical plastic piping used for drainage, was used due to its affordability and light weight. The pressure vessel consisted of a main body with a 7.6 cm interior diameter terminated on one end by a fixed cap and the other end terminated by a machined ABS flange. An end cap with an o-ring was bolted to this flange to provide the seal. The end cap was fitted with an epoxy-filled NPT threaded feedthrough, into which were fixed 4 wires, allowing for power and data transfer into and out of the vessel. The vessel is shown in Figure 10, and the performance of the pressure vessels during a rigorous thermal/vacuum test at NASA's Columbia Scientific Ballooning Facility (CSBF) in Palestine, TX is shown in Figure 11.

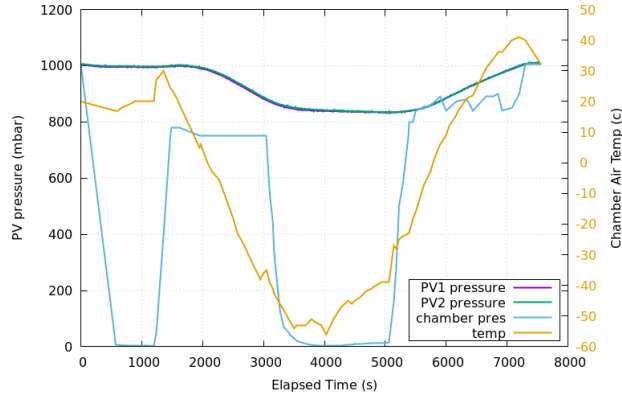Figure 10: The HiCal-2 pressure vessel.

Figure 11: Performance of the pressure vessel in a thermal/vacuum test, for which temperature and pressure were cycled through flight conditions. Note the dip in pressure due to the cold temperatures typical of ascent through the troposphere.

The antenna and HV system resided within the PV. Because the HiCal motor runs autonomously when powered and is not triggered or tied to a GPS clock, the pulse emission time is only predictable to within the ∼10 ms jitter in the camshaft rotation period, necessitating passive timestamping of the output pulses. To this end, a rigid 8 gauge pickup wire was threaded axially into the bicone, to detect the pulse and transmit it to the ATSA board (described below) for timestamping. The PV also housed a pressure monitor, to track the performance of the pressure vessel through the flight. The time-series data of the monitors for HiCal-2a (second HiCal balloon to be launched) and 2b (first HiCal payload to launch) are shown in Figure 12, showing that the PV integrity did not falter through the flight, and that it served as a de-facto thermometer, sensitive to the day/night cycle. The motor and the pressure monitor were both fed in parallel from a 5V source. Correspondingly, the 4 feedthrough wires through the endcap flange of the PV were power (5V), ground, pressure monitoring, and pulse pickup antenna for timestamping.
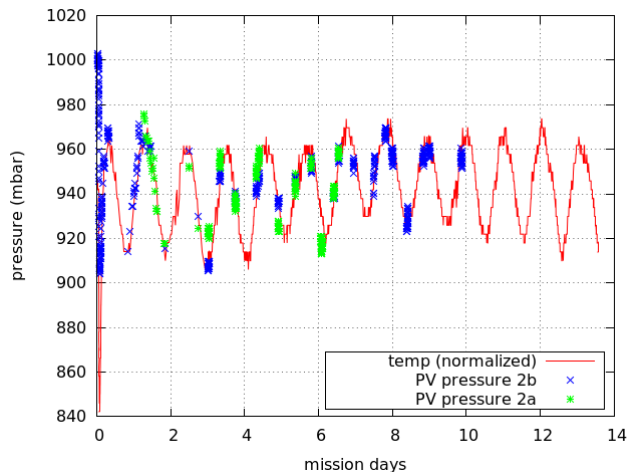
Figure 12: Pressure of the HiCal 2 PVs. For reference, the ambient temperature is overlaid, showing that the pressure tracks the ambient temperature, as it should at constant volume. The intermittent nature of the pressure vessel data is due to the operation of HiCal in flight. The instruments were activated for roughly 30 minutes, 3 times per day; pressure monitors are only powered at that time.

3.4. ATSA

The azimuth and time-stamp apparatus (ATSA), built in conjunction with the Moscow Engineering and Physics Institute (MEPhI), flew on top of HiCal-2 to provide azimuth information as well as timestamp information for the transmitted pulses. It consisted of a custom board governed by an ATMEL Atmega2560 microcontroller. The ATSA firmware monitored the timestamps from the pulser; a registered pulse would then latch the azimuth data and send it to the HiCal system board, which communicated with the NASA irridium communications system. The timestamp system had a resolution of 55μs, sufficient enough to isolate the HiCal events captured by ANITA by simple timestamp matching. The azimuth data, which was gathered by measuring the position of the sun using an array of 12 MEPhI designed- and produced silicon photomultipliers, was sent as a 1 byte word. As shown in Figure 13, the sensor was accurate to $\pm$ 3 degrees.
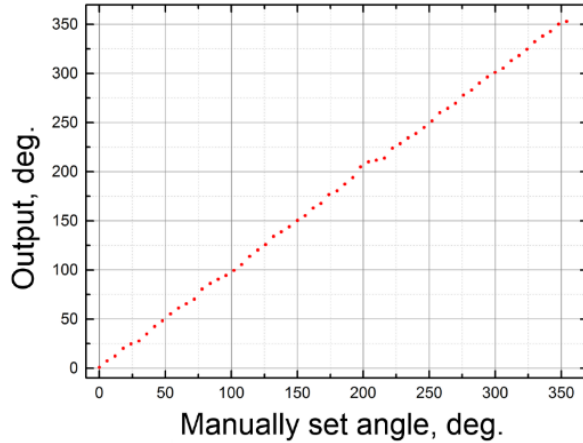
11

Figure 13: Actual sun position vs measured position for the ATSA sun-sensor unit (pre-flight data), indicating resolution of order 3 degrees.

3.5. HiCal system board

The HiCal system board was designed and built by the Instrumentation Design Laboratory (IDL) at KU. It featured a PIC microcontroller, and was responsible for formatting all of the science data for telemetery, and providing conditioned power to ATSA and the HV discharge system, including the PV pressure monitor. It included an internal clock, synced to GPS, that would latch when ATSA registered a pulse from the PV. This timestamp, along with temperature and azimuth, were formatted and sent via RS-232 to the NASA telemetery unit for each pulse.

3.6. NASA electronics and power

The NASA electronics, called the MIP, consisted of GPS and Iridium units, for position and telemetery purposes respectively. The instrumentation package on board HiCal-2 had a throughput of 255 bytes/minute, including 'housekeeping' data, such as GPS, temperature, and PV pressure monitoring, and 'science' data, including our timestamped pulses and azimuth information. The MIP also had commanding capability, which allowed us to remotely turn the system on and off through an electromechanical relay governing the power to the HiCal system board.

NASA also provided custom batteries for the instrument, designed specifically for the extreme conditions of flight. These batteries powered the MIP and HiCal electronics, via the aforementioned relay. Each payload had 2 battery packs.

4. Implementation and Testing

The systems were designed and built at various locations, but the implementation was performed over the summer of 2016 at CSBF. The CSBF facility

provides excellent diagnostic equipment and also access to the NASA Engineering staff. At the end of September 2016, a 'hang test' (Fig. 14) was performed where HiCal GPS and communication were tested, followed by shipment to Antarctica in mid-October, 2016.

Figure 14: The hang test at CSBF, where all systems performed nominally, verifying payload-readiness for the Antarctic flight.

5. Flight

HiCal-2b launched from NASA's Long Duration Ballooning Facility (LDB) on the Ross Ice Shelf of Antarctica on December 11 (leading ANITA-4 by approximately 700 km), with HiCal-2a launching on December 12 (trailing ANITA-

4 by approximately 500 km), roughly 10 days after ANITA 4 launched. Photos of the payloads just after launch are given in Figure 15. Although the original plan was to launch HiCal immediately after ANITA 4, logistics and weather made that impossible, requiring a delay until ANITA swung back close enough to LDB after its first revolution to allow a launch in proximity. Although both instruments performed well, one instrument died at one-half its expected lifetime – this may have been due to a failure in one of the battery packs, although the exact failure remains undiagnosed as the payloads were not recovered. Together the two payloads completed 1.5 cumulative revolutions of the continent for a combined 18 days of flight. Their flight paths are shown in Figure 16
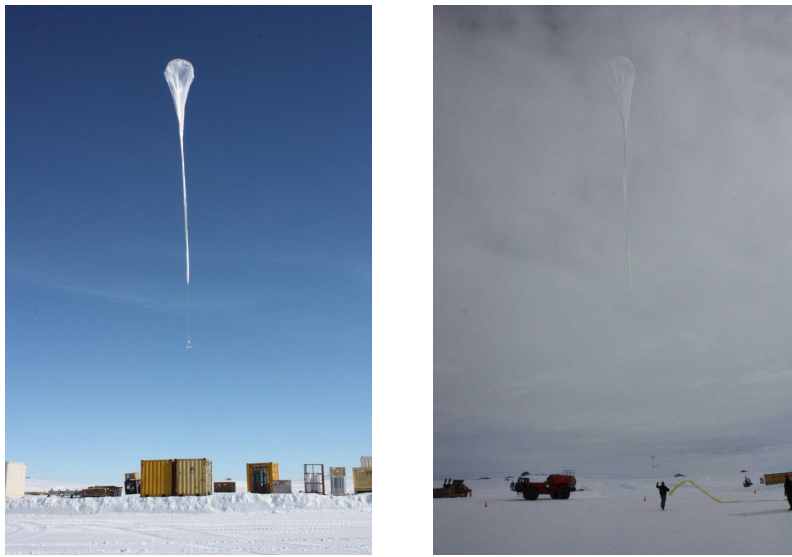

Figure 15: The two HiCal payloads, 2a and 2b, right and left respectively. HiCal-2b is barely visible against the backdrop of cloud cover.
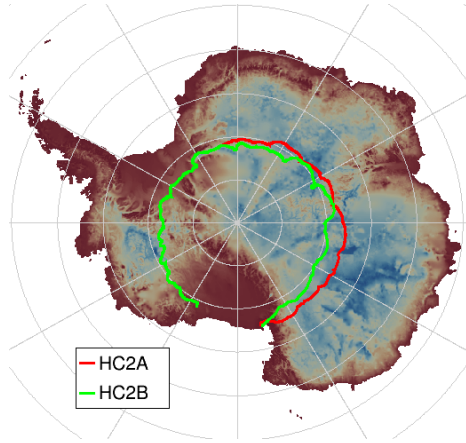
Figure 16: The HiCal flight paths during the ANITA4 flight.

6. Discussion and Outlook

The analysis of the HiCal-2 data is underway, and will be presented more completely in a companion article. Although designed to mimic the predominantly horizontally-polarized radio pulses from in-air cosmic ray interactions, initial analysis of ANITA data indicates that HiCal waveforms will have very little, if any utility as signal 'templates' for UHECR searches. The 10:1 HPol:VPol emitted power ratio further disfavors HiCal waveforms for neutrino searches, for which true signal should predominantly appear in Vertical polarization.

ANITA-4 captured $\mathcal{O}(10,000)$ pulses total, direct and reflected from the ice surface, from HiCal-2, with over 2,500 'pairs' analyzed thus far, for which both the direct and reflected impulses from the same pulse were recorded. An analysis of one of these pairs is given in Figure 17, showing the direct and reflected pulses as received by ANITA-4, with interferometric maps showing the angular reconstruction of the event as seen by the instrument. This dataset provides surface roughness information at observation angles (measured relative to the horizontal) of 4–23 degrees, and should therefore allow a high-statistics measurement of the surface roughness coefficient of the Antarctic ice.
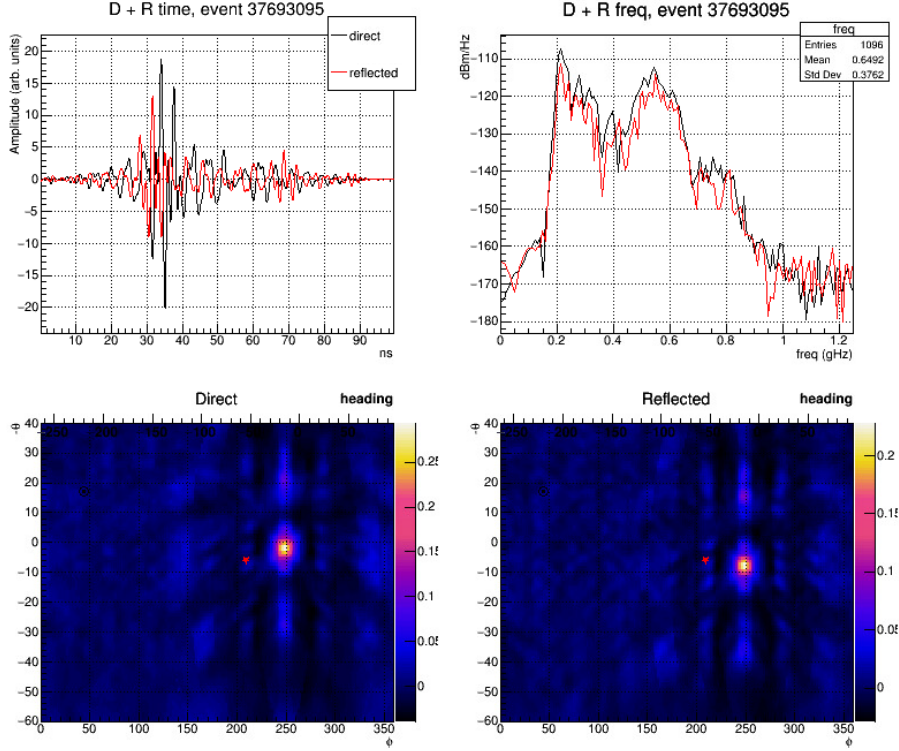
15

Figure 17: An example direct and reflected pair of a HiCal event as captured by ANITA. Clockwise from upper left, the time-series waveforms with the system response deconvolved, the power spectral density of both pulses, the interferometric map showing the source of the reflected event, and the interferometric map for the direct event.

HiCal-3, which is scheduled to fly with the proposed ANITA-5 instrument, will feature a larger payload, both horizontal and vertical polarizations, higher telemetry throughput, local RF pulse capture and improved time-stamping. This will allow us to have a record of the emitted pulse as well as the pulse as captured by ANITA, which will lower the systematic uncertainty in pulse-to-pulse variation during analysis.

7. Acknowledgments

References

[1] P. W. Gorham et al. The Antarctic Impulsive Transient Antenna Ultra-high Energy Neutrino Detector Design, Performance, and Sensitivity for 2006-2007 Balloon Flight. *Astropart. Phys.*, 32:10–41, 2009.

[2] G. A. Askar'yan. Excess negative charge of an electron-photon shower and its coherent radio emission. *Sov. Phys. JETP*, 14(2):441–443, 1962. [Zh. Eksp. Teor. Fiz.41,616(1961)].

[3] P. W. Gorham et al. Antarctic Surface Reflectivity Measurements from the ANITA-3 and HiCal-1 Experiments. *J. Astron. Inst.*, 06(02):1740002, 2017.

[4] H. Schoorlemmer et al. Energy and Flux Measurements of Ultra-High Energy Cosmic Rays Observed During the First ANITA Flight. *Astropart. Phys.*, 77:32–43, 2016.

[5] D. Z. Besson et al. Antarctic radio frequency albedo and implications for cosmic ray reconstruction. *Radio Science*, 50(1):1–17, 2015. 2013RS005315.